Available online at www.CivileJournal.org

Civil Engineering Journal

(E-ISSN: 2476-3055; ISSN: 2676-6957)

Vol. 11, No. 05, May, 2025

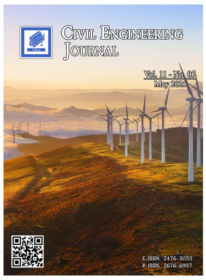

Flexural Behaviour of Prestressed Post-Tension Voided Biaxial Slab Under Uniformly Distributed Load

Ali Ahmed Hegab [1*], Magdy El-Sayed Kassem [1], Rasha T. S. Mabrouk [1]

[1] *Department of Structural Engineering, Faculty of Engineering, Cairo University, Giza 12613, Egypt.*

Received 15 December 2024; Revised 11 April 2025; Accepted 15 April 2025; Published 01 May 2025

Abstract

This study examines the flexural behavior of prestressed post-tensioned voided biaxial slabs under uniformly distributed loads (UDL) to evaluate structural performance, quantify material efficiency, and validate finite element models. Four full-scale slabs—solid and voided, with and without post-tensioning (PT)—were experimentally tested under UDL using a multi-level steel beam system to simulate uniform loading. Parameters such as crack initiation, deflection, and failure modes were monitored. Nonlinear finite element analysis (FEA) in ANSYS, employing Solid65 and Link180 elements, replicated material behavior and boundary conditions. The results showed that PT-voided slabs retained 96% of PT-solid yield capacity while reducing concrete volume by 22%, achieving a 21% self-weight reduction. Post-tensioning enhanced stiffness by 21% compared to non-PT voided slabs and delayed crack initiation. FEA predictions closely matched experimental data, with ≤10% deviation in load-deflection responses and consistent crack patterns. The novelty lies in demonstrating that PT effectively mitigates stiffness reductions (6% vs. PT-solid) caused by cuboidal voids, enabling high-performance, lightweight designs. This integration of PT with voided systems offers a sustainable solution, reducing material usage by up to 22% while maintaining structural integrity, thereby advancing eco-efficient construction practices. Findings provide critical insights for optimizing voided slab applications in modern infrastructure.

Keywords: Voided Slabs; Post Tension Slab; Prestress Concrete; ANSYS.

1. Introduction

Voided slabs were developed several decades ago, initially aimed at minimizing the self-weight of concrete slabs. Initially, one-way voided slabs were developed to achieve this objective, using materials such as foam, tar paper, metal, hollow tiles, sonotubes, and slag block to introduce voids in the slab's longitudinal direction [1]. However, these systems exhibited significant variations in load-carrying capacity along orthogonal directions, making them most suitable for unidirectional floor slabs. Later, systems using ribbed slabs, such as waffle and joist slabs, were developed to overcome this restriction. In 1997, Cobiax, a specialized voided former manufacturer, developed an environmentally efficient, lightweight hollow body system [2]. Around the same time, Danish structural engineer Jorgen Breuning created Bubble Deck technology; it represented the first biaxial hollow slab that was practical [3]. Subsequently, in 2001, the modular U-Boot element was introduced to reduce transportation costs through its stackable design, which allows for efficient packing and minimizes delivery trips to construction sites [4].

Biaxial voided slabs are reinforced concrete slabs incorporating plastic void formers—typically spherical, donut-shaped, or cuboid—positioned between reinforcing meshes at the top and bottom. This leads to a 50%

* Corresponding author: alihegab@cu.edu.eg

http://dx.doi.org/10.28991/CEJ-2025-011-05-09

reduction in self-weight when compared to traditional reinforced concrete solid slabs, without significantly altering structural performance [5]. By reducing self-weight, the demands on other structural elements, such as foundations and columns, are lessened, leading to a reduced need for materials like reinforcement and concrete by up to 15% [4].

Examples of structures using voided slabs with post-tension systems can be seen in New York City's Columbia University Medical Center Graduate Education Building (CUMGEB) (Figure 1), with an area of about 9,290 m² and standing as a 15-story tower characterized by geometric complexities. One of the main structural challenges was to achieve reduced structural depth and extended open floor spans while adhering to deflection performance criteria for the all-glass façade. The structure features cascading sections with no exterior columns, resulting in a distinctive arrangement of cantilevered flat plate slabs with voids. These slabs have a bonded post-tensioning reinforcement system to meet performance requirements, with Cobiax void formers positioned between post-tensioning bands to facilitate extended span, beam-like framing using flat formwork and reduced self-weight. High-strength concrete is used in these cantilevered slabs, which taper from 0.6 m at the supports to 0.2 m at the free ends [6].

Claremont, California's Harvey Mudd College Teaching and Learning Building (Figure 1) holds the distinction of being the first university building in the U.S. to adopt BubbleDeck technology of voided slabs. Completed in 2013, this four-story, 7,400 m² structure features an innovative approach to seismic weight reduction, essential for its location within a region prone to high seismic activity. The structural engineering team employed voided slabs in the design, incorporating five different sizes of void formers, ranging from 0.23 to 0.5 m. This resulted in a reduction of 570 m³ of concrete. The decreased self-weight enabled the use of more slender shear walls and reduced the floor-to-floor height for the 10-meter clear spans. This structural system was preferred by both the owner and the architectural team, as the exposed flat soffit of the semi-precast slab and the voids facilitate easier future renovations.

Figure 1. CUMCGEB Voided Slab Cantilevered Flat Plate (left), Harvey Mudd College Semi-Pre-Cast Voided Slab Construction (right)

Recent advancements in voided slab systems have focused on optimizing structural efficiency while reducing material consumption, driven by the need for sustainable construction practices. A predominant research direction centers on void geometry optimization, where diverse configurations—including spherical (Bubble Deck systems) [7], ellipsoidal [8], cuboidal [9, 10], donut-type [11], and conical voids [12]—have been systematically evaluated for their structural implications.

Sagadevan & Rao [9] conducted a comparative analysis of spherical and cuboidal void geometries in one-way slabs, concluding that both shapes resulted in comparable stiffness reductions. Khouzani et al. [8] examined shear behavior using ellipsoidal voids, while Pawar et al. [10] explored flexural performance in biaxial voided slabs with cuboidal voids, observing that increased void size reduced stiffness and ultimate load capacity, precipitating slab failure. Chung et al. [11] demonstrated the efficacy of donut-type voids in enhancing flexural strength and stiffness, whereas Bhamare et al. [12] proposed conical voids as a novel geometry for optimizing slab stiffness.

These studies emphasize the critical relationship between void morphology and mechanical performance, particularly in mitigating stress concentrations and enhancing load distribution [10, 13]. For instance, cuboidal voids have demonstrated superior compatibility with flexural reinforcement, while conical geometries propose potential stiffness enhancements [10, 12]. Such investigations aim to balance material efficiency with structural functionality, addressing inherent trade-offs in voided systems.

Further investigations into void configuration and spacing have employed parametric analyses to refine load capacity and flexural behavior. Key variables include void size, spacing, and the void-width-to-spacing ratio (b/s) [10, 14]. Sagadevan and Rao [15] used uniform and staggered void distribution in biaxial reinforced concrete (RC) slabs, concluding that void shape minimally influences flexural capacity, as the neutral axis resides within the cover concrete above the top reinforcement. Pawar et al. [10] prioritized uniform void distribution to minimize localized stress gradients, ensuring homogeneous load transfer across the slab.

Experimental and computational methodologies further dominate investigations into structural behavior under loading. Sagadevan & Rao [15] used sixteen-point loading systems to simulate uniformly distributed loads (UDL) in physical tests, while analytical methods such as Yield Line Theory [9] and Finite Element Analysis (FEA) in ABAQUS [7] and ANSYS [16, 17] validate results and extrapolate parametric trends. These approaches collectively quantify flexural capacity [9], shear resistance [18], and deflection limits, revealing failure modes unique to voided systems, such as premature cracking near void peripheries [10].

To counteract structural vulnerabilities, innovative reinforcement strategies have emerged. Techniques such as embedding steel bars through voids [10], implementing steel cages [13], and utilizing composite reinforcement bars [17] aim to enhance flexural performance and ductility while reducing steel consumption. Such methods aim to reconcile the trade-off between material efficiency and structural robustness, ensuring voided slabs meet safety standards without compromising sustainability goals.

Beyond structural optimization, comparative studies benchmark voided slabs against conventional solid slabs, demonstrating reduction in self-weight while retaining comparable load capacities. Jain and Hussain [19] conducted numerical investigations, revealing that voided slabs achieved over 15% weight reduction compared to conventional slabs, alongside a construction cost reduction exceeding 10%. However, stiffness reductions and increased deflections—partially mitigated through optimized void geometries—highlight the need for careful design calibration [13, 15].

Emerging research explores advanced methodologies to expand voided slab applications. Machine learning frameworks predict punching shear strength reduction factors, offering data-driven design insights [20]. These innovations reflect a shift toward standardized, computationally aided design protocols.

While PT is well-established in solid slabs, its application to biaxial voided slabs remains underexplored. Prior research lacks empirical data on how PT interacts with cuboidal voids to mitigate stiffness reductions and cracking in biaxial systems, particularly under uniformly distributed loads (UDL).

2. Research Significance

The increasing demand for efficient and sustainable construction solutions has led to seeking for innovative solutions to improve structural efficiency and sustainability. Among these, voided slab systems have gained significant attention due to their potential for material savings and improved structural performance. However, the behavior of prestressed post-tensioned biaxial voided slab systems has not been investigated so far.

This research aims to fill the existing knowledge gap through conducting experimental and numerical investigations on full-scale prestressed post-tensioned voided slab specimens to evaluate the appropriateness of these provisions on the flexural capacity. Figure 2 shows a flowchart of the research methodology. The specific objectives of this study are to:

- Evaluate the flexural capacity and stiffness of voided slab systems compared to solid slab systems under uniformly distributed loads.
- Quantify the material savings achieved through the use of voided slab systems.
- Validate the accuracy of finite element analysis (FEA) models in predicting the behavior of prestressed post-tensioned voided slabs.
- The findings of this research will contribute to the following:
- Advancement of knowledge: By providing experimental data and numerical simulations, this research will enhance the understanding of the flexural behavior of prestressed post-tensioned voided slabs.
- Improved design practices: The results will enable engineers to design more efficient and economical prestressed concrete structures.
- Sustainable construction: By promoting the use of voided slab systems, this research can contribute to reducing the environmental impact of construction.

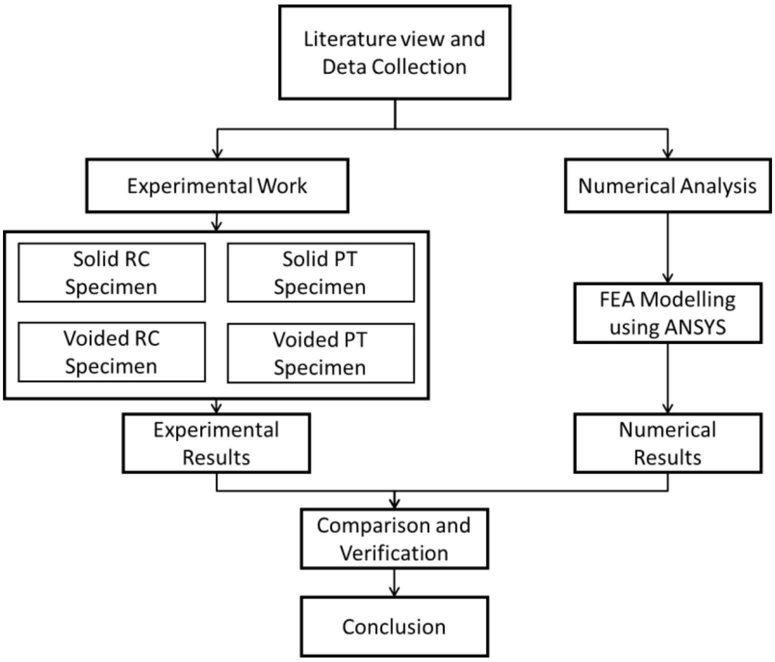

Figure 2. Research methodology flow chart

3. Experimental Setup

3.1. Details of Test Specimens

Due to laboratory equipment constraints and rigid frame dimensions, a total of four full-scale slab specimens, each measuring 2200 mm × 2200 mm × 160 mm, were subjected to experimental testing. These specimens were designed to study the influence of specific parameters, namely the presence of voids and prestressed reinforcement, on the structural behavior of RC slabs. To ensure the validity and relevance of the experimental results, the specimens were configured to replicate real-world conditions, specifically those encountered in typical RC residential buildings. The specimens were regarded as a part of a prototype flat slab with equal spans. Each span is about 3.5 meters in length to ensure that the outer lines of the slab specimens were bounded by the lines of moment contra-flexure (zero moment lines). Figure 3 illustrates a moment diagram exhibiting contra-flexure points. The reinforcement arrangement, comprising both longitudinal and transverse reinforcement, was carefully selected to prioritize flexural behavior over shear failure, a common concern in voided slab systems. The reinforcement bars were 8 mm in diameter, configured in a mesh pattern at 150 mm spacing to provide adequate tensile strength, with a clear cover of 12 mm and an average cover of 20 mm measured from the slab soffit and top of concrete for the bottom and top mesh, respectively. The most commonly used strand diameters are 12.7 mm and 15.2 mm. In our specimen, which featured a slab thickness of 160 mm, the 12.7 mm strands were selected. Furthermore, a mono post-tensioning strand system was implemented to adequately accommodate the 50 mm rib spacing between voids. Additionally, a minimum average pre-compression exceeding 0.9 MPa was adopted, in accordance with the minimum post-tensioning requirements specified in prevalent design codes. A detailed summary of the dimensions of the specimens, reinforcement details, and void configurations is presented in Table 1. The specimens' details are shown in Figures 4 to 7.

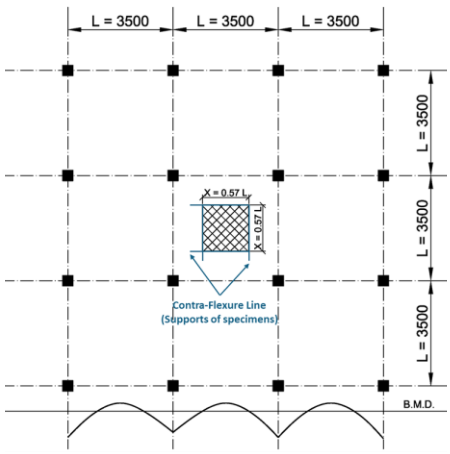

Figure 3. Prototype of the flat slab

Table 1. Geometry and reinforcement of the specimens

Specimen	Type	Dimensions (mm)	RFT	PT
1	Solid RC	2200×2200×160	15Ø8 Top & Bottom	-----
2	Voided RC			
3	Solid PT			2 × 12.7 mm Strands at each direction
4	Voided PT			

(a) RC Solid specimen (b) RC Voided specimen

Figure 4. Formwork, steel and void formers for the RC specimens

(a) PT Solid specimen (b) PT Voided specimen

Figure 5. Formwork, steel and void formers for PT specimens

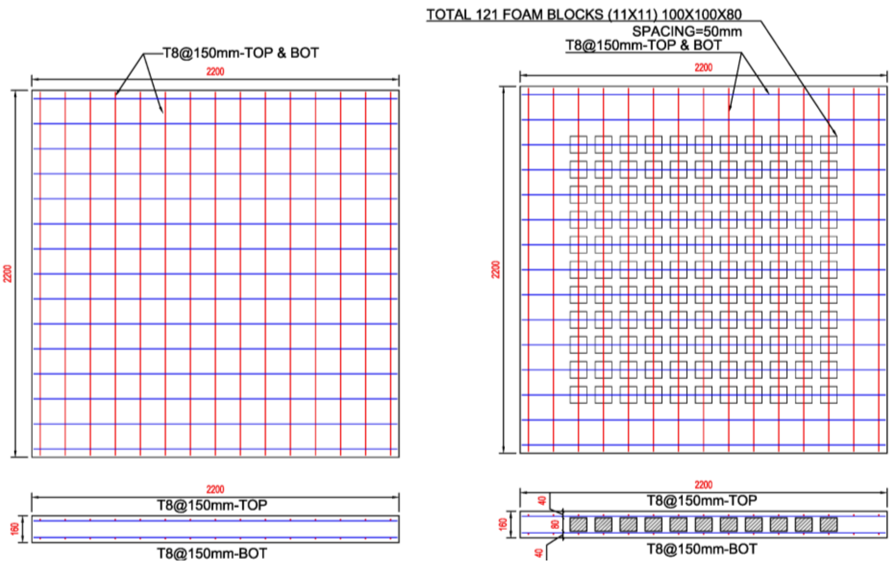

(a) RC Solid specimen (b) RC Voided specimen

Figure 6. PT, steel and void arrangement for the RC specimens

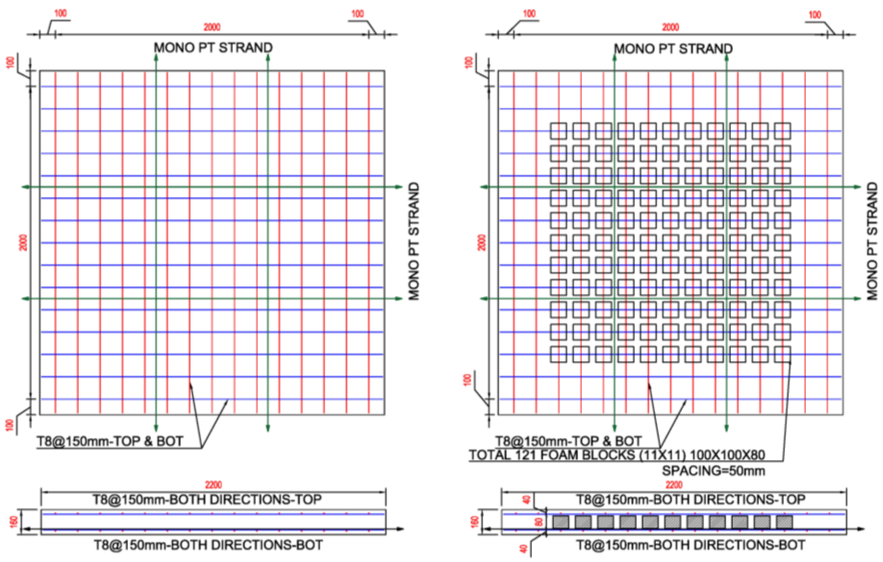

(a) PT Solid specimen (b) PT Voided specimen

Figure 7. PT, steel and void arrangement for PT specimens

3.2. Void Formers

Lightweight polystyrene cubes (100 mm × 100 mm × 80 mm) were employed as void formers to create a regular pattern of voids within the slab. These cubes were strategically positioned with a clear spacing of 50 mm in both directions. To ensure adequate concrete cover and prevent potential bond failures, the void formers were elevated using 10 mm spacers, maintaining a consistent clear cover of 40 mm at both the top and bottom surfaces of the slab. The cuboid void former dimensions and its photograph are shown in Figure 8.

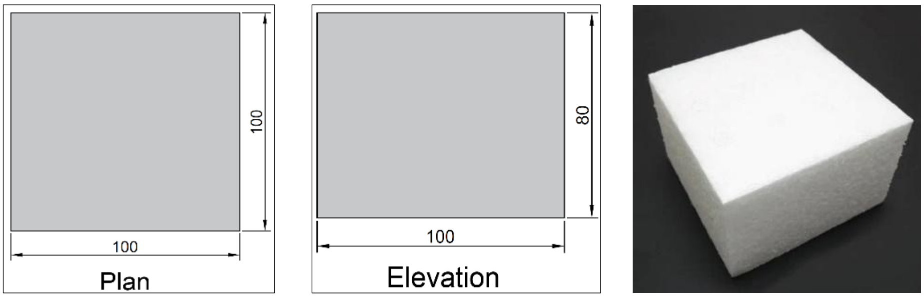

Figure 8. Cuboid void former

3.3. Materials

The concrete mix utilized for the test specimens was designed to reach a compressive strength of 28 MPa at 28 days. The maximum particle size of the coarse aggregate was restricted to 10 mm, while the fine aggregate was limited to a maximum particle size of 5 mm. This selection of aggregate sizes ensures optimal packing density, enhancing the concrete's strength and durability as a whole. The results from the sieve analysis conducted on fine and coarse aggregates are shown in Figure 9.

For flexural reinforcement, high-grade rebars of 8 mm diameter were incorporated into the specimens. These rebars, classified as 520 grade steel, possess exceptional mechanical qualities, ensuring high ductility and high tensile strength.

For post-tensioning, 12.7 mm diameter, seven-wire, high-carbon, low-relaxation PT strands were used. These strands exhibit high tensile strength (1860 MPa) and yield stress of (1700 MPa). Plastic ducts with a diameter of 2 cm were used to house the post-tensioning tendons, ensuring their proper alignment and protection.

Finally, mono cast iron anchors and wedges were utilized to secure the post-tensioning tendons to the concrete. These components play a crucial role in transferring the tensile forces from the tendons to the concrete, thereby enhancing the overall structural performance of the specimens. Table 2 summarize the material properties of the used Reinforced Concrete (compressive strength) and flexural reinforcement.

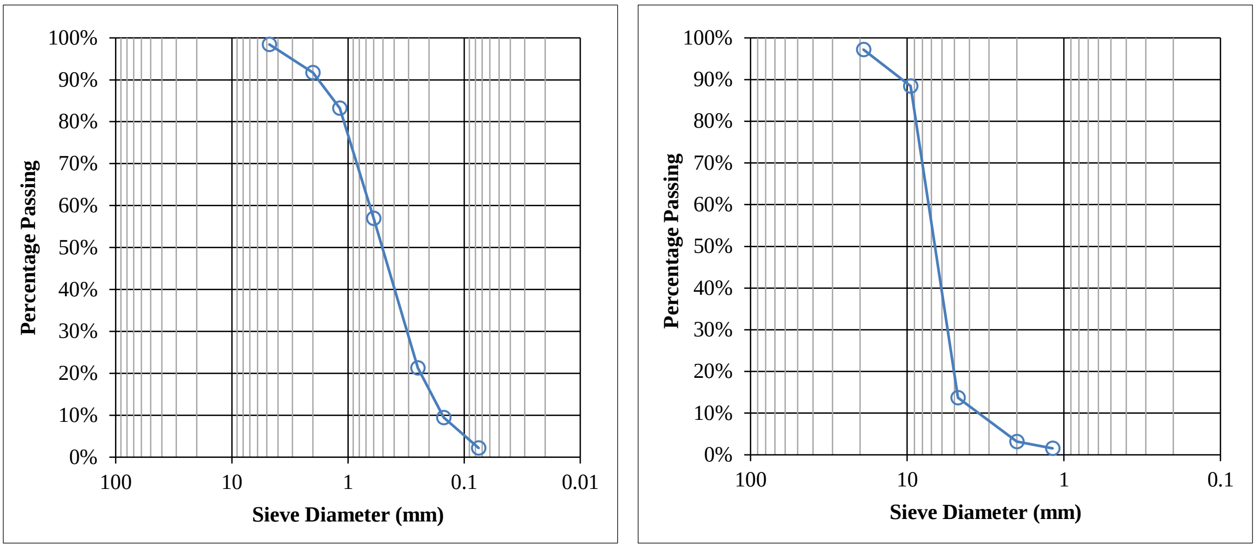

(a) Fine Aggregates (b) Coarse Aggregate

Figure 9. Sieve Analysis Results for used Aggregates

Table 2. Used materials, properties and characteristics

Material	Characteristics
Concrete	Cubic compressive strength at 28 days, f_{cu}=28 MPa
Flexural reinforcement	High-grade steel 360/520 of diameter 8 mm
PT Strands	12.7 mm PC Strand 7-Wire High Carbon Tensile Strength Low Relaxation (f_{py}=1700 MPa, f_{pu}=1860 MPa)
Void former	Lightweight high density polystyrene cubes (32 kg/m^3)
Ducts	Plastic ducts of 2 cm diameter
Anchors	Mono cast iron anchor and wedge

3.4. Casting of the Test Specimens

The mixing process of concrete was conducted in a ready-mix patch plant and delivered using a concrete mixer truck. The concrete was compacted using a mechanical vibrator, and the concrete surface was finished using a steel tool. The slab specimens were covered by wet burlap for a period of seven days and kept wet during the curing process. Meanwhile, the concrete cubes were kept submerged in the water during the curing process until the testing day. Figure 10 shows the pouring process of concrete.

Figure 10. Pouring process of concrete

After the concrete has gained sufficient strength, the post-tensioning (PT) cables, also known as tendons, are then stressed using mono hydraulic jacks as shown in Figure 11, which apply tension to the cables. Following the tensioning, the elongation in the strand was measured. In addition, the dial gauge reading was recorded to ensure transferring the calculated force, as shown in Figure 12. After achieving the required force and elongation in strands, the ducts are grouted to achieve a full bond between the strand and casted concrete, as shown in Figure 13.

Figure 11. PT cables stressing using mono hydraulic jack

Figure 12. Measuring elongation in PT cables

Figure 13. Grouting to achieve full bond between strand and casted concrete

3.5. Test Setup

A specialized steel system consists of 15 steel beams on 4 levels, shown in Table 3. Each transformation level was guided by steel angles to ensure the stability of the load transfer system. This system has been designed to transform the concentrated point load exerted by a hydraulic jack into a distributed load. This is achieved by applying pressure to 16 equal areas at the 4th level, effectively simulating a uniform load distribution. The design ensures that the load is evenly spread across the structure, reducing the risk of localized stress concentrations and potential structural failures. The use of multiple pressure points allows for a more accurate representation of real-loading conditions. Figure 14 shows the test setup and specimen installation.

Table 3. Loading system levels and used steel sections

Level	Steel Section
1	Built-up steel beam (box section), with 3 internal stiffeners at load application and transfer locations
2	Two (HEA 340) steel beams, with 3 stiffeners at load application and transfer locations
3	Four (SHS 200×5) steel beams, with 3 stiffeners at load application and transfer locations
4	Eight (SHS 200×5) steel beams, with 2 legs from same section, each ended by a plate (220x200x10 mm)

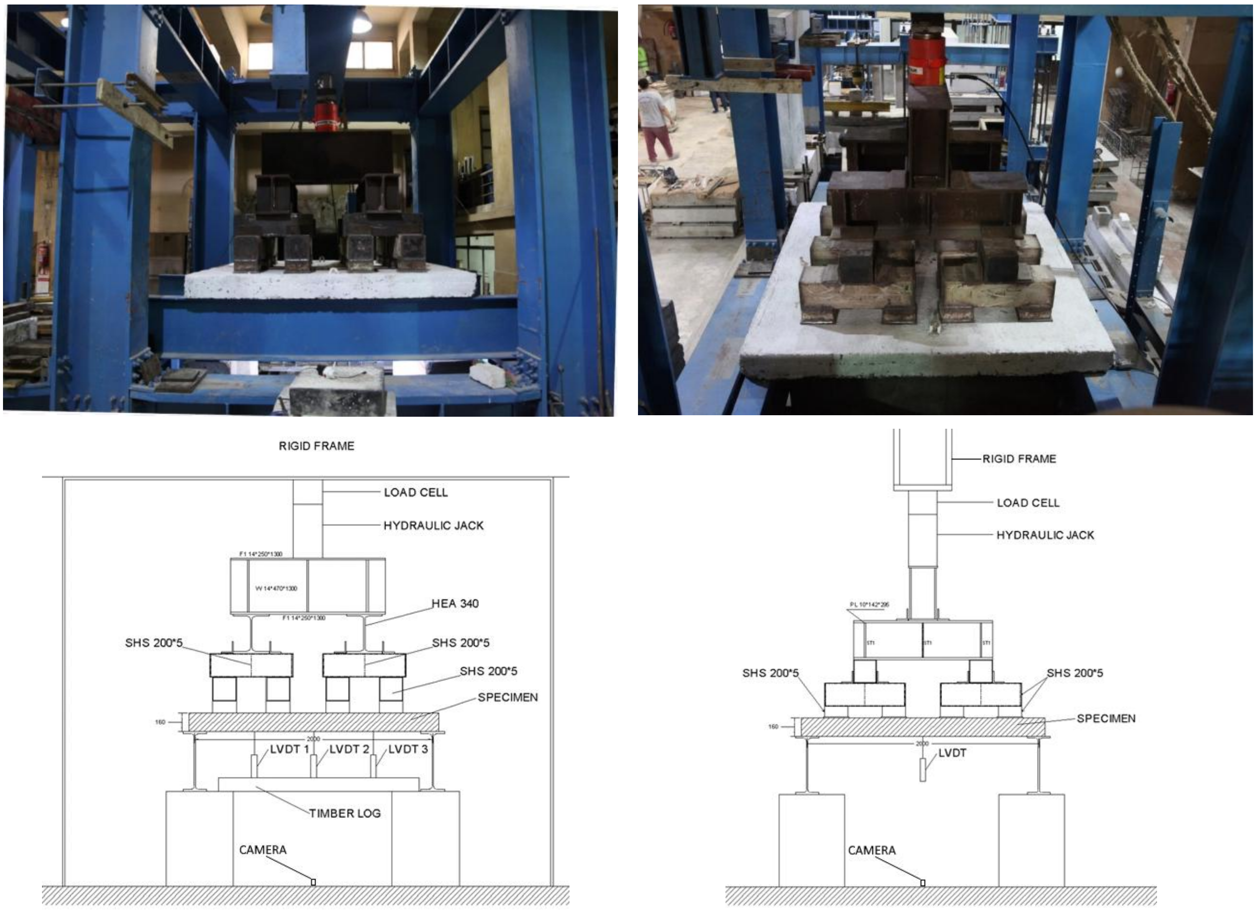

Figure 14. Test setup and specimen installation (a & b)

To comprehensively monitor the behavior of the specimens, a combination of load cells, Linear Variable Differential Transformer (LVDT) sensors, strain gauges, and cameras have been installed. A load cell is used to record the load at each load step corresponding to other measurements. LVDT sensors are employed to measure precise displacements and deformations of the specimens. Strain gauges, on the other hand, are employed to monitor the strain within the bottom reinforcement mesh to record the first yield. Additionally, high-resolution cameras are utilized to visually document the specimens' behavior, capturing real-time images and videos that can be analyzed to identify any visible cracks, deformations, or other anomalies.

After installing the specimen on the supporting frame and installing *LVDT*s, the hydraulic jack was installed. Subsequently, the load cell, *LVDT*s, and the strain gauges were attached to the data logger system by electrical wires. The capacity of the loading actuator is 2000 kN, and the capacity of the load cell is 1350 kN.

Specimens were loaded with the mentioned load increment till failure or reaching the capacity of the hydraulic jack. And the loading process was being held when cracks appeared to be monitored and marked on the specimen.

4. Results and Discussion

4.1. Crack Patterns

Initial surface flexural cracks typically formed at the mid-span region. These cracks appeared earlier in voided slabs compared to solid slab specimens. As the load increased and the reinforcement began to yield, diagonal cracks initiated from the mid-span and propagated toward the outer edges. Subsequently, additional cracks developed, predominantly in a diagonal direction. At the ultimate loading stage, these diagonal cracks expanded and coalesced, forming an X-shaped failure pattern resembling yield lines. While this pattern was consistent across all four specimens, voided specimens exhibited additional square-shaped cracks reflecting the void and rib distribution. It is important to note that the specific crack widths and propagation rates varied among the four specimens.

In the RC solid specimen, cracks propagated uniformly with a typical X-shaped failure pattern, displaying moderate widths due to the absence of void-induced stress concentrations. The RC voided specimen, however, exhibited additional square-shaped cracks corresponding to the void and rib layout, along with less uniform crack propagation influenced by the void arrangement. For the post-tensioned solid specimen, initial cracks were delayed and appeared at higher loads due to the enhanced stiffness provided by post-tensioning. In contrast, the post-tensioned voided specimen also delayed crack initiation but exhibited distinct square-shaped cracks linked to the void distribution, with crack widths and propagation rates lying between those of the RC voided and post-tensioned solid specimens. Figures 15 and 16 show the crack patterns at the tension side for the specimens.

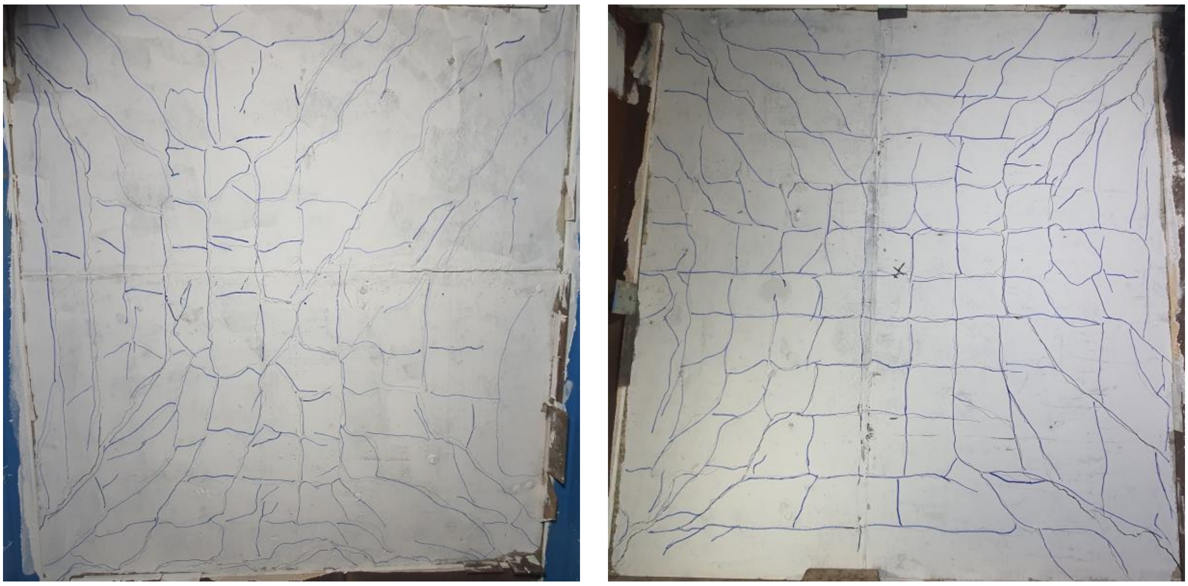

(a) RC Solid specimen (b) RC Void specimen

Figure 15. Crack pattern for the RC specimens

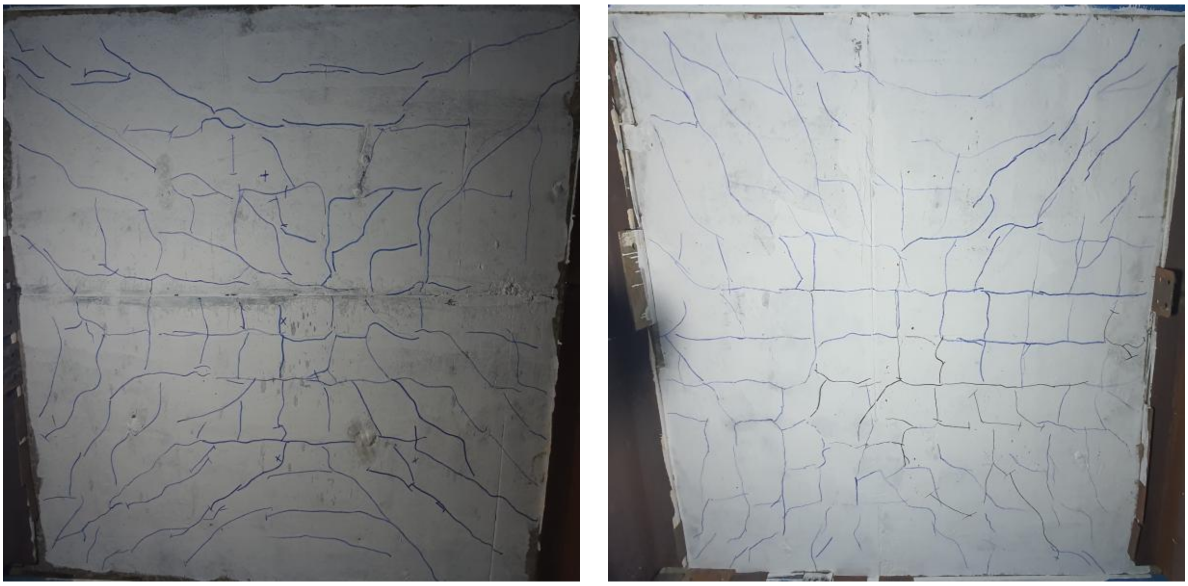

(a) PT Solid specimen (b) PT Void specimen

Figure 16. Crack pattern for the PT specimens

Among the four tested specimens, the RC-Voided specimen was the only one to reach failure under the applied load. Its mode of failure was characterized by flexural failure, with diagonal cracks expanding and coalescing into an X-shaped pattern, accompanied by additional square-shaped cracks reflecting the void and rib distribution. The cracks propagated extensively until the specimen could no longer sustain the applied load, ultimately failing at 1090 kN with a corresponding deflection of 20.8 mm.

The remaining three specimens (RC-Solid, PT-Solid, and PT-Voided) did not fail but instead reached the hydraulic jack's capacity of 1350 kN. These specimens exhibited superior load-carrying capacity due to either the absence of voids or the enhancement provided by post-tensioning. If failure had occurred, it would likely have been dominated by flexural mechanisms, as indicated by the observed X-shaped crack propagation at ultimate loads. Notably, the post-tensioning in the PT-Solid and PT-Voided specimens significantly delayed crack initiation and reduced crack widths, contributing to their high resistance and preventing complete failure within the jack's capacity. Both PT-Voided and PT-Solid slabs exhibited similar X-shaped flexural failure modes. Although the PT-Voided slabs exhibited additional square-shaped cracks reflecting the void distribution, there were no indications of premature failure.

4.2. Deflection

For all specimens, the deflection shows a linear relationship with the applied load up to the point of initial cracking, which occurs at loads of 320, 350, 500, and 550 kN for the Voided RC, Solid RC, Voided PT, and Solid PT specimens, respectively. The corresponding deflections at cracking are 2.2, 2.7, 3.2, and 3.1 mm. After the onset of cracking, the stiffness of the specimens decreases due to crack propagation, leading to a reduction in the slope of the load-deflection curve and a transition to nonlinear behavior. In this phase, the flexural reinforcement on the tension side begins to yield at loads of 850, 950, 1200, and 1250 kN, with corresponding deflections of 10.7, 11.7, 12.5, and 12.3 mm for the Voided RC, Solid RC, Voided PT, and Solid PT specimens, respectively. Table 4 summarizes the load-deflection results for the specimens. The load-deflection behavior at various loading stages is illustrated in Figure 17. Additionally, the load corresponding to the initial yielding of the flexural reinforcement on the tension side is marked on each curve as a small triangle.

Table 4. Load deflection results

Specimen	First Crack		First Yield		Ultimate Load	
	Load (Pcr); kN	Deflection (Δcr); mm	Load (Py); kN	Deflection (Δy); mm	Load (P_{ult}); kN	Deflection (Δ_{ult}); mm
S1 (RC-Solid)	350	2.7	950	11.7	1300*	22.3
S2 (RC-Void)	320	2.2	850	10.7	1090	20.8
S3 (PT-Solid)	550	3.1	1250	12.3	1300*	11.9
S4 (PT-Void)	500	3.2	1200	12.5	1300*	14.3

* Specimen's failure did not occur; maximum recorded values are limited by the load cell's capacity.

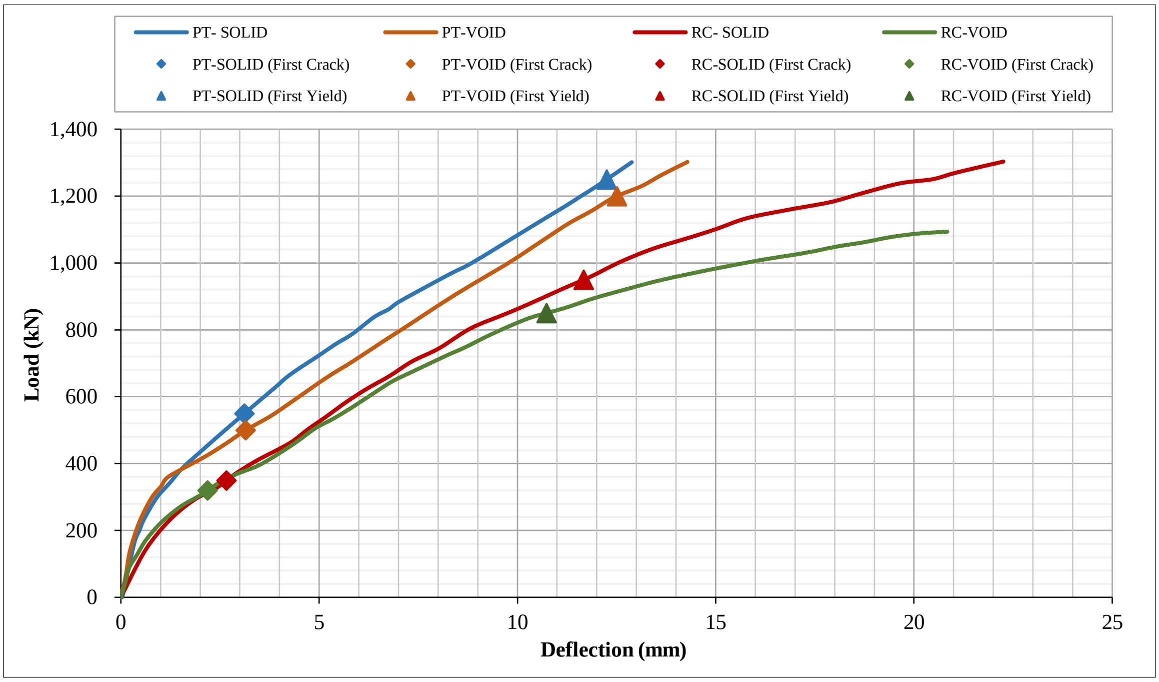

Figure 17. Load vs. deflection behavior for specimens

4.3. Flexural Capacity and Stiffness

Slab Flexural stiffness is defined as the ratio between the applied load to the corresponding mid-span deflection. Applying the aforementioned rule at the yield load (Py) with its corresponding deflection (Δy), secant stiffness (Ky) will be determined [15, 21].

The flexural stiffness values for the specimens were 79, 81, 96, and 102 kN/mm for the Voided RC, Solid RC, Voided PT and Solid PT specimens, respectively. RC-Void specimens have a 3% lower secant stiffness than RC-Solid specimens, attributed to the reduction in the effective cross-sectional area due to the voids in the slab. PT-Void specimens had 6% less secant stiffness than PT-Solid specimens.

To further discuss the results from the tests, the tested specimens are grouped into two groups: Group 1 includes the PT specimens (PT-Solid and PT-Void), and Group 2 includes the non-PT specimens (RC-Solid and RC-Void) to compare their behavior.

In Group 1, the PT-Voided slab showed slight performance reductions compared to the PT-Solid slab due to the inclusion of voids. Crack patterns in the PT-Solid specimen were uniform and X-shaped, with delayed initiation due to its continuous material and enhanced stiffness from post-tensioning. The PT-Void specimen, while showing similar crack propagation, displayed additional square-shaped cracks reflecting the void distribution. The first crack load of the PT-Voided slab was slightly lower (500 kN vs. 550 kN for PT-Solid), and its deflection at cracking was slightly higher (3.2 mm vs. 3.1 mm). Similarly, the PT-Voided slab achieved 96% yield load capacity of the PT-Solid slab (1200 kN vs. 1250 kN), with corresponding deflections of 12.5 mm and 12.3 mm, respectively. Stiffness comparisons show a modest 6% reduction for PT-Voided slabs (96 kN/mm vs. 102 kN/mm). However, the PT-Voided slab achieves this near-equivalent performance with 22% less material, highlighting its efficiency.

In Group 2, behavior followed a similar trend as seen in Group 1. Crack patterns in the RC-Solid slab were uniform and X-shaped, while the RC-void slab exhibited square-shaped cracks due to the void layout, with less uniform propagation. The first crack load for the RC-Void slab was slightly lower (320 kN vs. 350 kN for RC-Solid), with deflections of 2.2 mm and 2.7 mm, respectively. Yielding behavior followed a similar trend, with the RC-Solid slab yielding at 950 kN (11.7 mm deflection) and the RC-Voided slab yielding at 850 kN (10.7 mm deflection), achieving 89% yield load capacity. Stiffness comparisons show a 3% reduction in the RC-Voided slab (79 kN/mm vs. 81 kN/mm for RC-Solid).

When comparing the PT-Void slab to the RC-Void slab, the benefits of post-tensioning become evident. Both slabs exhibited additional square-shaped cracks reflecting the voids, but the PT-Voided slab showed delayed crack initiation and smaller crack widths due to enhanced stiffness from post-tensioning. The first crack load for PT-Void was significantly higher at 500 kN compared to 320 kN for RC-Void, with deflections of 3.2 mm and 2.2 mm, respectively. Similarly, the PT-Void slab outperformed the RC-Void slab in yield load (1200 kN vs. 850 kN) and deflection at yield (12.5 mm vs. 10.7 mm), showing improved structural resistance (41% yield load improvement) and deformation control. The stiffness of PT-Void (96 kN/mm) was 20% higher than RC-Void (79 kN/mm), illustrating that post-tensioning effectively compensates for the stiffness reductions caused by voids. These findings highlight the ability of PT-Voided slabs to combine material efficiency with enhanced performance, making them a superior choice for sustainable structural designs.

4.4. Finite Element Analysis

To gain deeper insights into the complex behavior of two-way voided slabs, a nonlinear finite element (FE) analysis was conducted using ANSYS 15 software.

In this study, the concrete was modeled using an eight-node solid element (Solid65). This element was selected because it effectively captures key behaviors such as plastic deformation, cracking in three directions (x, y, and z), and crushing.

Link180 elements were employed to model the steel reinforcement rebars and post-tension tendons. These elements require two nodes and possess three degrees of freedom per node for translations in the x, y, and z directions. Similar to the concrete element, Link180 can represent plastic deformation in the steel. A 3D mesh with fine elements, having a maximum uniform size of 10 mm, was employed to model each slab.

The modeling and simulation of the flexural behavior of prestressed biaxial voided slabs in ANSYS followed a systematic approach to ensure accuracy and reliability. Material properties for concrete and prestressing steel were precisely defined. A fine mesh was employed to enhance precision, while simply supported boundary conditions were applied to replicate experimental setups. Prestressing was modeled as an initial strain of 0.006 in the post-tensioning elements. Nonlinear analysis accounted for material and geometric nonlinearity. The Newton-Raphson iterative solver was utilized, employing linearization and iterative updates to achieve convergence. This process involves making an initial guess, approximating the equations with a Taylor series expansion around this guess, and then iteratively updating the solution. Incremental loading was applied to stabilize the solution and capture progressive behaviors like crack propagation, yield onset, and ultimate failure. Concrete samples were taken during casting the specimens and tested to get the maximum compressive strength. That compressive strength was then used in the modeling of the nonlinear concrete material model in ANSYS. The compressive behavior of concrete was defined using a nonlinear stress-strain curve, while tensile behavior assumed linear elasticity until cracking, followed by tension softening with reduced stiffness. Post-cracking shear transfer coefficients ($\beta_t = 0.3$ for open cracks, $\beta c = 0.9$ for closed cracks) were specified to account for interlock effects. The modelling process utilized the actual characteristic concrete compressive strength determined from cube testing. The concrete tensile strength was considered to be $0.6\sqrt{f_c'}$ as per ACI 318-19 [22]. Poisson ratio used for concrete was assumed to be 0.2 while 0.3 was used for steel. Additionally, the concrete's elasticity modulus was considered as $4700\sqrt{f_c'}$(MPa).

The geometry, applied load, and node locations of the elements are shown in Figure 18. The material properties for used in the model are shown in Table 5. Stress distribution of the bottom rebars mesh at yield stress, and the top stresses distribution in concrete just before crushing failure for the RC-Solid Specimen are shown in Figure 19-a and 19-b.

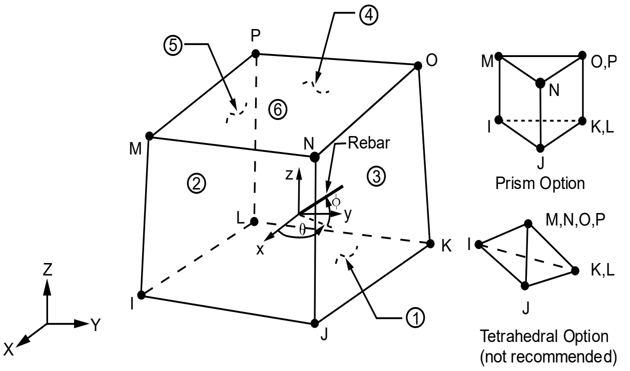

(a) SOLID65 Element

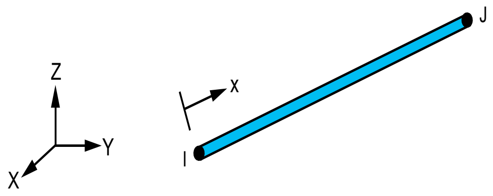

(b) LINK180 Element

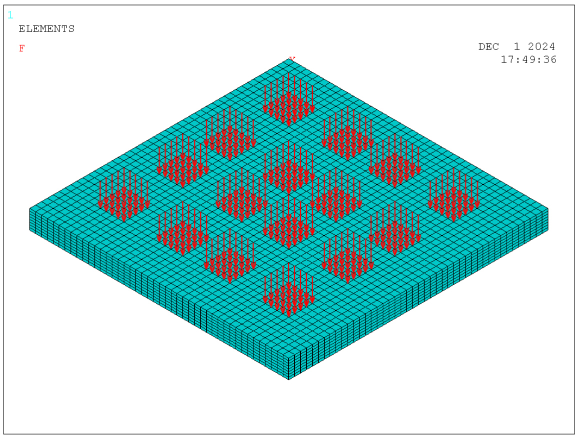

(c) Applied Load

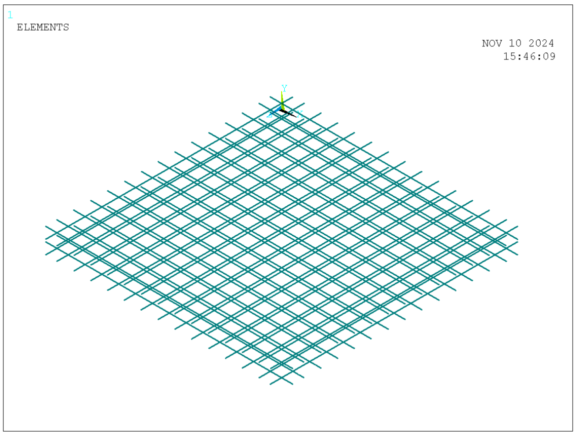

(d) Rebar Mesh

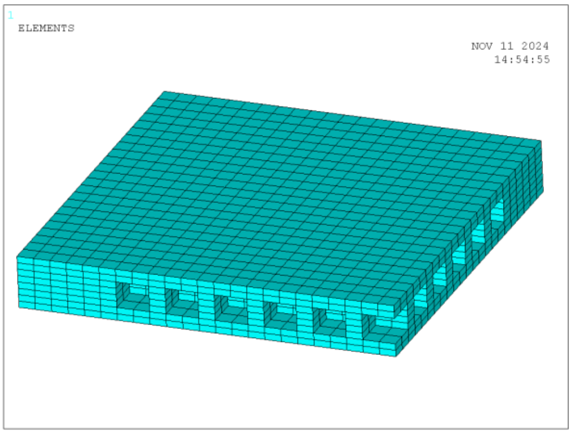

(e) Voided Slab

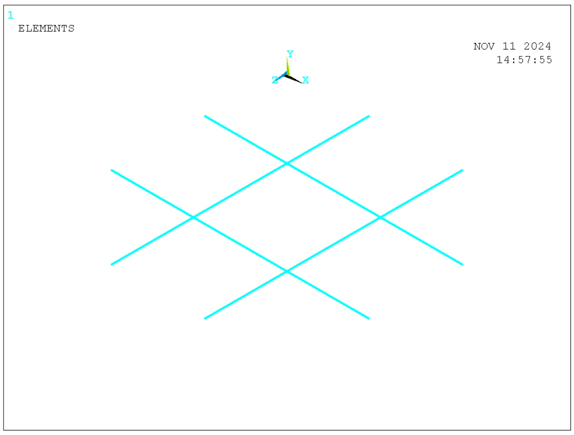

(f) PT Tendons

Figure 18. Elements used for modelling concrete, steel rebars and PT tendons

Table 5. Materials properties parameters

Material Type	**Mechanical Characteristics**	
Concrete	Young's modulus of elasticity	E = 24870 MPa
	Poisson's ratio	$\upsilon = 0.2$
	Ultimate compressive strength	$f_c = 28$ MPa
	Concrete tensile strength	$f_{ctr} = 3.2$ MPa
	Open shear transfer coefficient	$\beta_t = 0.3$
	Closed shear transfer coefficient	$\beta_c = 0.9$
Steel	Yield strength	$f_y = 520$ MPa
	Young's modulus of elasticity	$E = 2 \times 10^5$ N/mm^2
	Poisson's ratio	$\upsilon = 0.3$
PT-Steel	Yield strength	$f_y = 1700$ MPa
	Young's modulus of elasticity	$E = 2 \times 10^5$ N/mm^2
	Poisson's ratio	$\upsilon = 0.3$

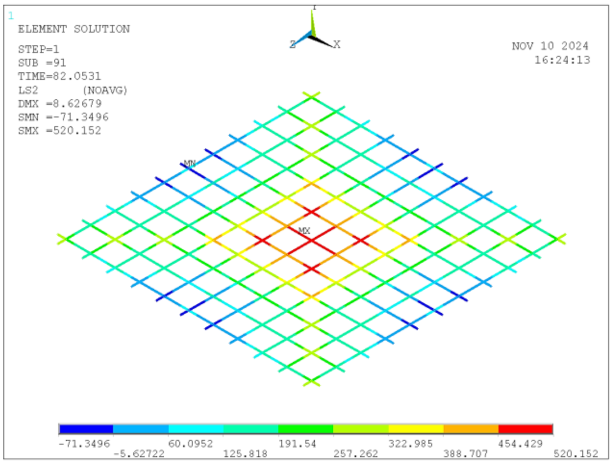

(a) Stress in bottom rebars at yield

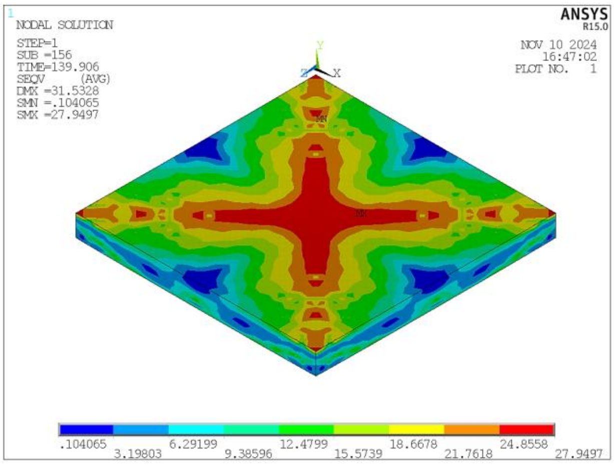

(b) Stress in concrete top surface at failure

Figure 19. Stresses distribution in rebars and concrete

The analytical study using ANSYS is conducted to validate the accuracy and reliability of the numerical model against the experimental results presented in this work. The main objective is to ensure that the ANSYS model accurately captures the behavior of the tested slabs, including load-deformation characteristics, crack patterns, and failure modes. By comparing the numerical predictions with experimental data, the validity of the model can be assessed, establishing confidence in its use for further analysis.

This validation is critical because the analytical model serves as the foundation for future parametric studies that will be explored in subsequent research. Once validated, the ANSYS model can be used to simulate various design scenarios and investigate the effects of key parameters, such as void size, shape, spacing, reinforcement configuration, and post-tensioning configuration. These parametric studies will enable a deeper understanding of the structural performance of voided and post-tensioned slabs under different conditions, providing valuable insights for optimizing their design and application in construction.

4.5. Finite Element Analysis Results

Figure 20 shows how the load and deflection at the midspan relate in the finite element models, while Figure 21 compares these results with experimental data, highlighting a strong similarity between the two methods. The load-deflection behavior was almost identical, with both following the same pattern—starting with similar initial stiffness up to the yielding stage, then showing minor variations as they approached the ultimate load. Table 6 provides a summary of the numerical analysis results alongside those from the tested specimens.

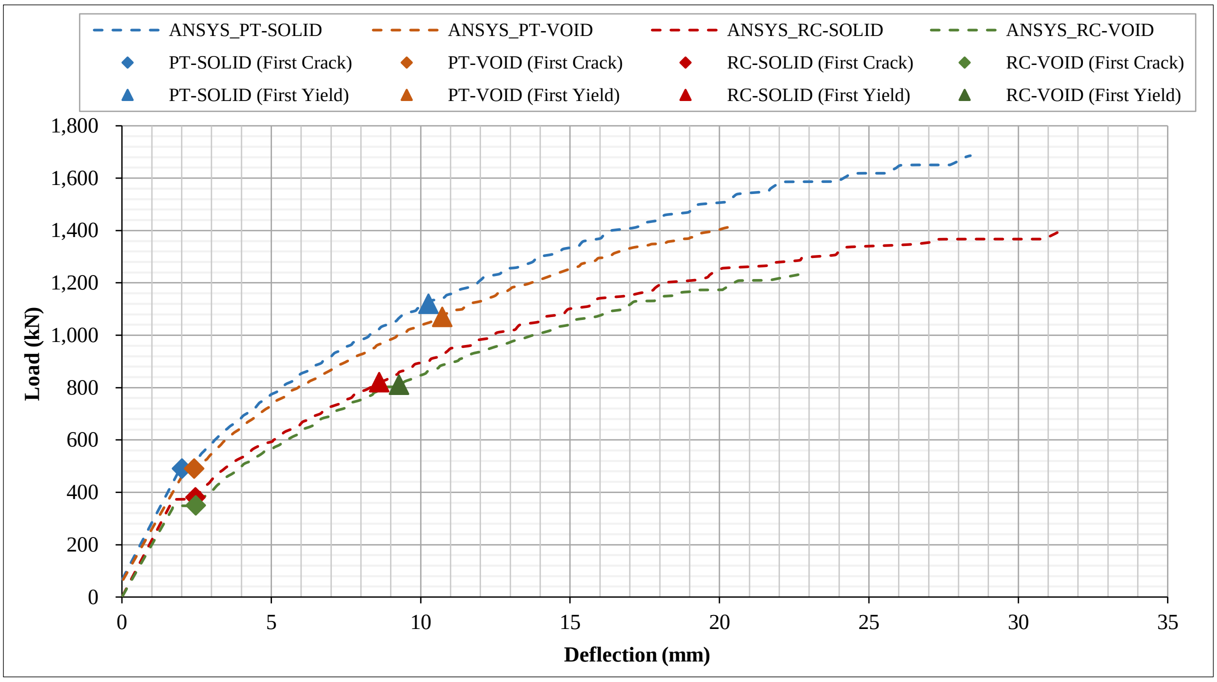

Figure 20. Load vs deflection behavior for the numerical models

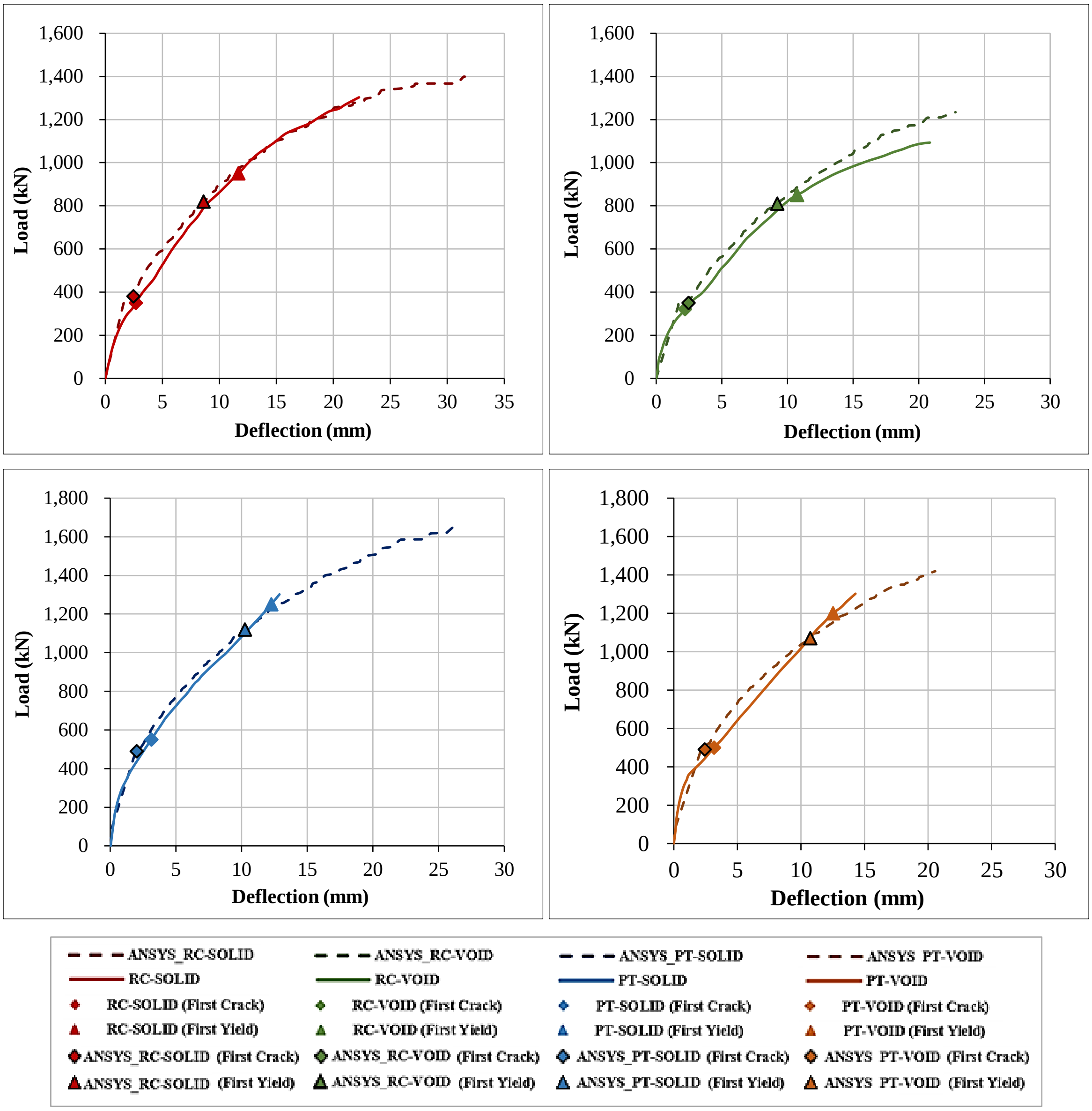

Figure 21. Load vs. deflection behavior for experimental and numerical models

Table 6. Comparison between experimental and numerical results

Specimen	Experimental						FEA Numerical (ANSYS)					
	First Crack		First Yield		Ultimate Load		First Crack		First Yield		Ultimate Load	
	(Pcr) kN	(Δcr) mm	(Py) kN	(Δy) mm	(P_{ult}) kN	(Δ_{ult}) mm	(Pcr) kN	(Δcr) mm	(Py) kN	(Δy) mm	(P_{ult}) kN	(Δ_{ult}) mm
RC-Solid	350	2.7	950	11.7	1300*	22.3	380	2.5	820	8.6	1399	31.5
RC-Void	320	2.2	850	10.7	1090	20.8	350	2.5	810	9.3	1234	22.8
PT-Solid	550	3.1	1250	12.3	1300*	11.9	490	2.0	1120	10.3	1686	28.3
PT-Void	500	3.2	1200	12.5	1300*	14.3	490	2.4	1070	10.7	1419	20.6

* Specimen's failure did not occur; maximum recorded values are limited by the load cell's capacity

4.6. Crack Pattern

The ANSYS program captures the crack patterns corresponding to each applied load increment. Crack patterns from the finite element models are shown in Figures 22 to 25. The red-colored regions in the ANSYS visualization highlighted the locations of cracking and crushing, further validating the model's ability to replicate the physical behavior of the tested slabs under increasing loads. The failure modes observed in the finite element models align closely with the experimental slab data and corresponding observations, showing flexural failure characterized by the development and propagation of cracks. As the load increased, the cracks first appeared in the mid-span region, reflecting tensile stress in the concrete. These cracks propagated diagonally towards the edges as the reinforcement yielded, forming an X-shaped failure pattern.

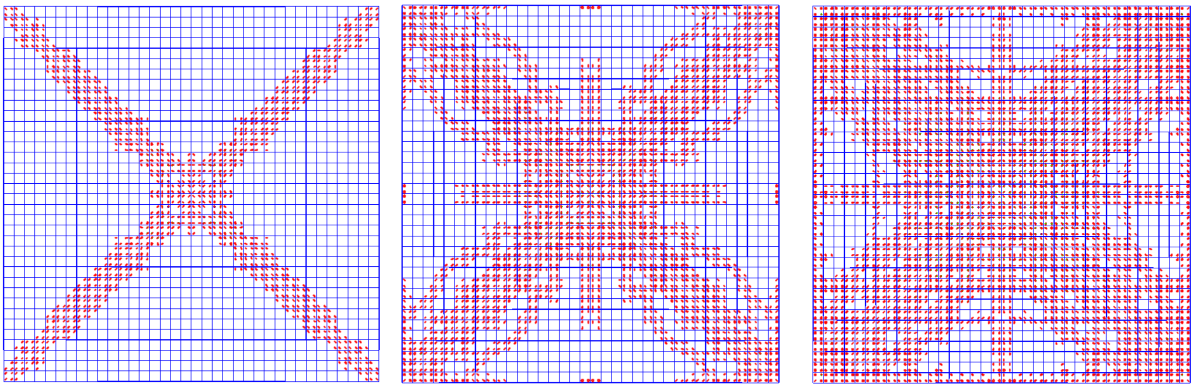

(a) First Crack (380 kN) (b) Crack propagation (600 kN) (c) Crack at yield (820 kN)

Figure 22. RC-Solid FE model crack initiation and propagation

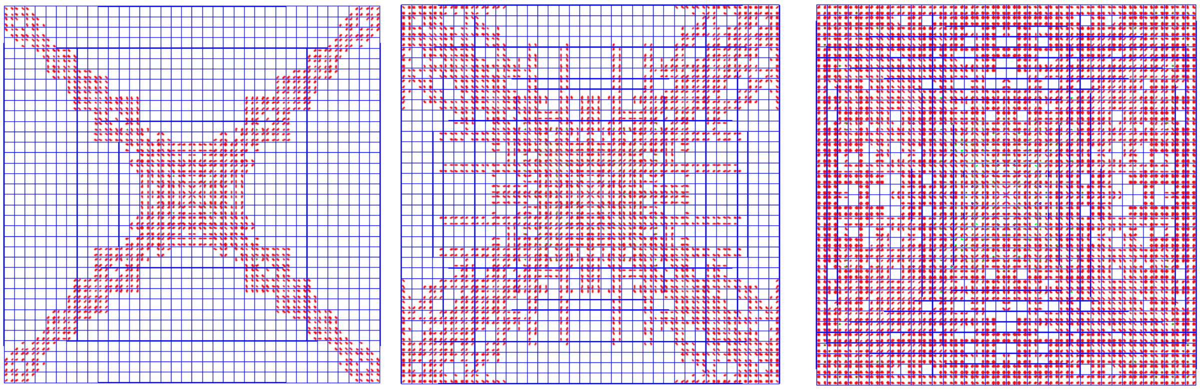

(a) First Crack (350 kN) (b) Crack propagation (581 kN) (c) Crack at yield (810 kN)

Figure 23. RC-Void FE model crack initiation and propagation

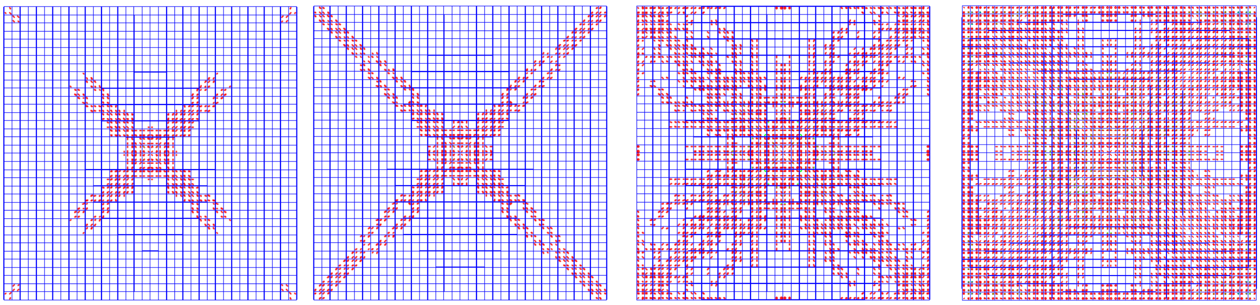

(a) First Crack (490 kN) (b) Crack propagation (530 kN) (c) Crack propagation (800 kN) (d) Crack at yield (1120 kN)

Figure 24. PT-Solid FE model crack initiation and propagation

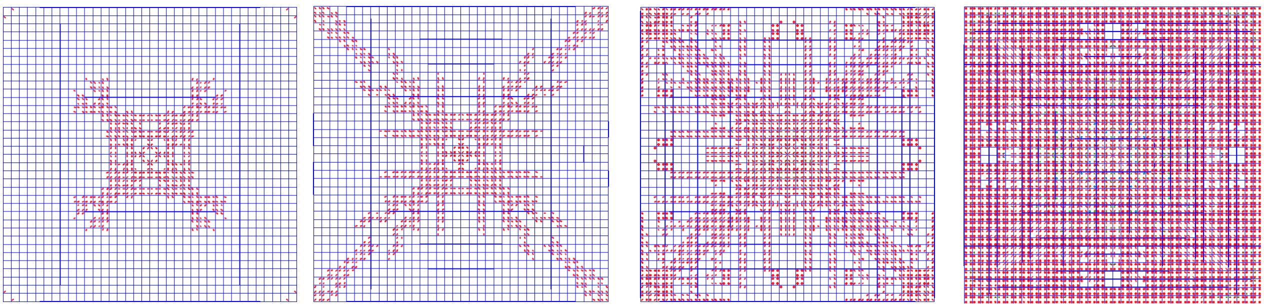

(a) First Crack (490 kN) (b) Crack propagation (530 kN) (c) Crack propagation (800 kN) (d) Crack at yield (1120 kN)

Figure 25. PT-Void FE model crack initiation and propagation

The Finite Element Analysis (FEA) results were categorized into two groups for comparative analysis: Group 1, comprising the post-tensioned (PT) slabs (PT-Solid and PT-Voided), and Group 2, consisting of the non-post-tensioned (RC) slabs (RC-Solid and RC-Voided).

In Group 1, the FEA results for the PT-Solid and PT-Voided slabs demonstrated strong alignment with experimental data, affirming the efficacy of post-tensioning in offsetting the performance reductions induced by voids. Both specimens displayed a first crack load of 490 kN. However, the PT-Voided slab exhibited slightly higher deflection at the cracking stage (2.4 mm) compared to the PT-Solid slab (2.0 mm). After the initiation of cracking, the cracks propagated to form an X-shaped pattern, typical of flexural behavior under loading. However, in the voided slab, additional cracks appeared more scattered, reflecting the influence of the ribs and void distributions. The resulting square-shaped cracks, corresponding to the void layout, indicate the redistribution of stresses within the slab and emphasize the structural interactions between the solid concrete regions and voided areas. At the yield stage, the PT-Voided slab achieved 95.5% of the yield load capacity of the PT-Solid slab (1070 kN versus 1120 kN). Stiffness evaluations indicated an 8% reduction for the PT-Voided slab compared to the PT-Solid slab, with stiffness values of 100 kN/mm and 108 kN/mm, respectively.

In Group 2, the RC-Solid and RC-Voided slabs in the FEA exhibited similar behavioral trends to those observed experimentally. The RC-Voided slab experienced cracking earlier (350 kN) than the RC-Solid slab (380 kN), with both exhibiting an initial deflection of 2.5 mm. At the initial stage of crack formation, the cracks in both slabs exhibited an X-shaped pattern, typical of flexural failure under loading. However, in the voided slab, the cracks were wider and displayed a less uniform shape compared to the solid slab. As the load increased, the cracks propagated further; additional cracks reflecting ribs and voids layout became evident in the voided slab. Yield load capacities were 820 kN for the RC-Solid slab and 810 kN for the RC-Voided slab, corresponding to deflections of 9.3 mm and 8.6 mm, respectively. The stiffness of the RC-Voided slab was 8% less than that of the RC-Solid slab, with values of 87 kN/mm and 95 kN/mm, respectively.

Comparing the PT-Void slab to the RC-Void slab reveals notable differences in crack behavior despite both slabs exhibiting additional square-shaped cracks corresponding to the voids' layout. The PT-Void slab demonstrated delayed crack initiation as a result of the increased stiffness imparted by post-tensioning. Furthermore, the cracks in the PT-Void slab were narrower and more controlled compared to the RC-Void slab. This reduction in crack width highlights the superior ability of post-tensioning to resist tensile stresses and mitigate crack propagation, contributing to improved structural integrity and enhanced durability of the voided slab system. The first crack load for the PT-Void slab was significantly higher (490 kN) compared to the RC-Void slab (350 kN), while their respective deflections were 2.4 mm and 2.5 mm. At yield, the PT-Voided slab significantly outperformed the RC-Voided slab, achieving a yield load of 1070 kN (versus 810 kN) and a deflection of 10.7 mm (versus 9.3 mm), demonstrating a 32% improvement in yield load. The stiffness of the PT-Void slab (100 kN/mm) was 15% higher than the RC-Void slab (87 kN/mm), illustrating that post-tensioning effectively compensates for the stiffness reductions caused by voids.

The FEA results were found to align closely with the experimental data, validating the numerical model's ability to predict the flexural behavior, crack patterns, and modes of failure of the specimens. Both the experimental and numerical results showed that post-tensioning significantly enhances the performance of voided slabs, improving their stiffness, load-bearing capacity, and crack resistance. The analytical models accurately captured the critical behaviors, such as first crack loads, yield loads, and deflections, confirming that post-tensioning in PT-Voided slabs compensates for the stiffness reductions associated with voids. Additionally, the crack patterns observed in the FEA were consistent with those observed in the experiments, validating the model's ability to simulate real-world slab behavior under load. Figures 26 and 27 show the crack pattern from the experimental results compared to the FEA models.

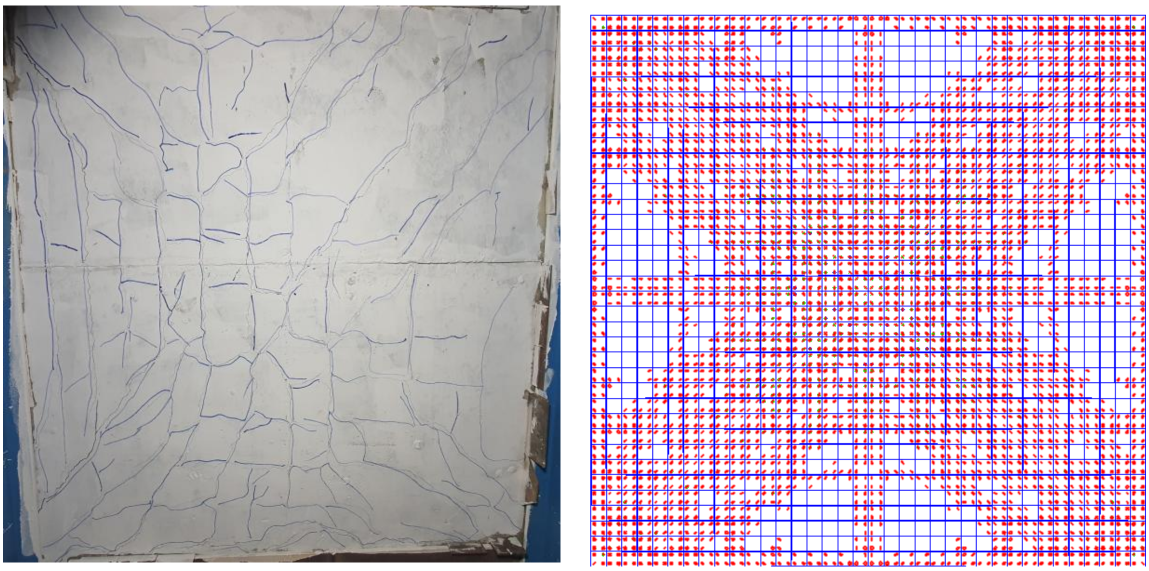

(a) RC-Solid specimen

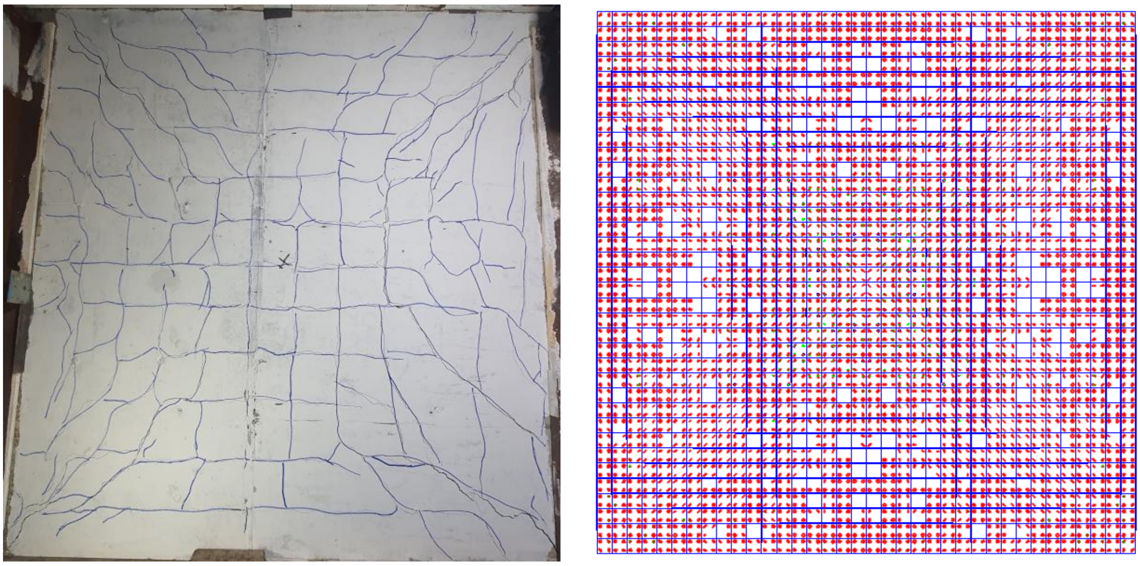

(b) RC-Void specimen

Figure 26. RC specimens crack pattern comparison (experimental vs. analytical)

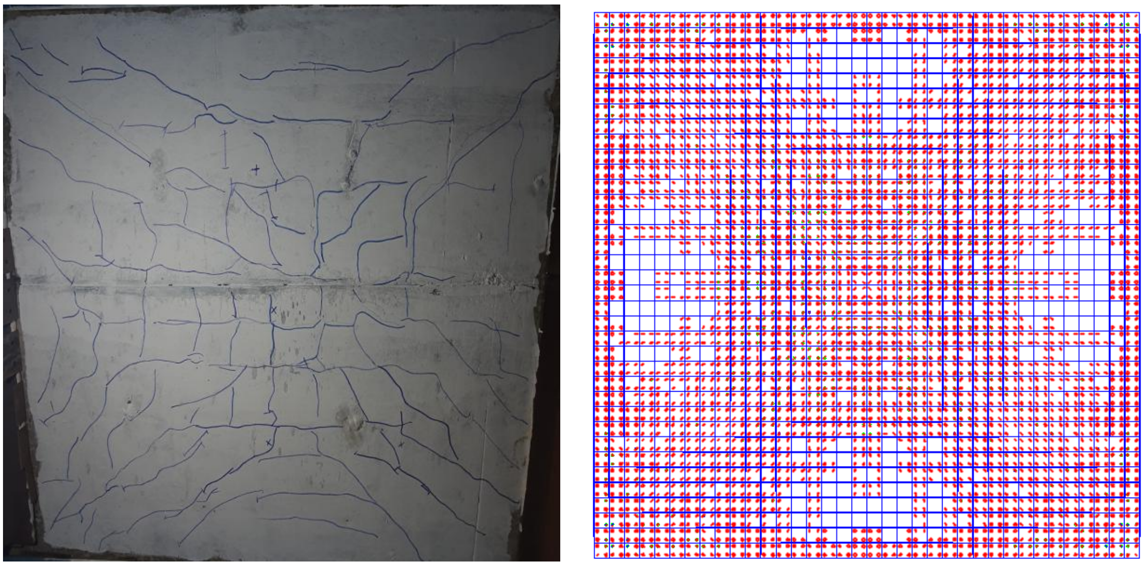

(a) PT-Solid specimen

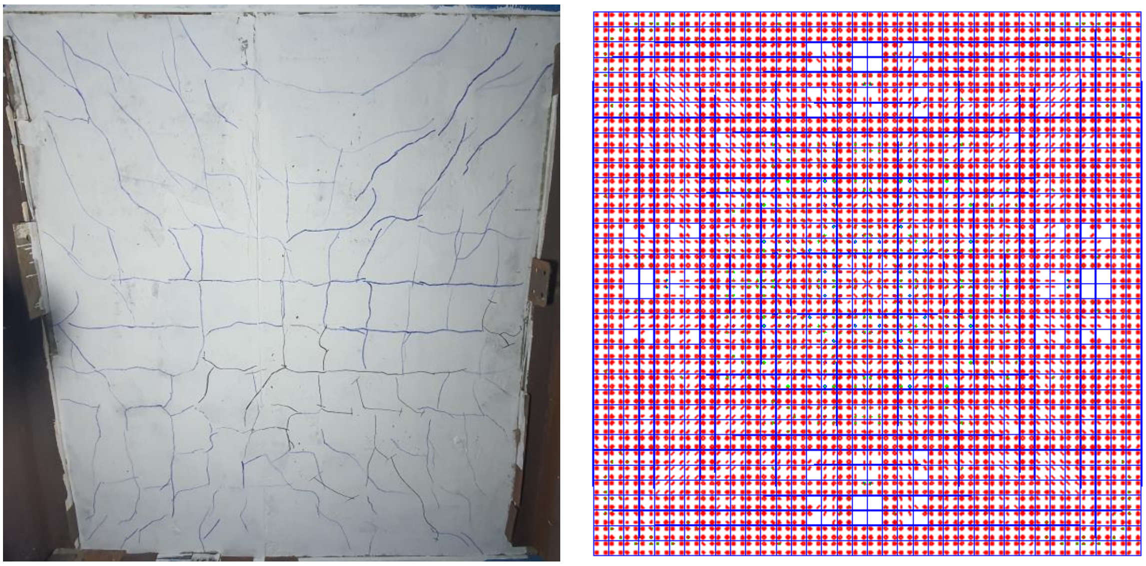

(b) PT- Void specimen

Figure 27. PT specimens crack pattern comparison (experimental vs. analytical)

4.7. Comparing the Results with Experimental Studies from the Literature

First Yield Load: The experimental investigations consistently demonstrated that voided slabs achieve flexural capacities comparable to those of solid slabs, with nuanced variations influenced by design parameters. Since three of the four tested specimens did not reach their ultimate capacity and, to the authors' knowledge, no prior research has investigated the use of post-tension in voided slabs, direct comparisons focus on the yield load of the non-post-tensioned voided slab with the values reported in the literature. In this study, the reinforced concrete (RC) voided slab retained 91% of the yield load capacity of the conventional RC solid slab, even though the concrete volume was reduced by 22%. Similarly, Pawar et al. [10] observed only minor reductions (1–9%) in yield load capacity for voided slabs with cuboidal voids, despite variations in void dimensions. In contrast, the experimental study by Sagadevan & Rao [15] reported that voided slabs maintained 117% of the yield load capacity of solid slabs, attributing this performance largely to the beneficial effects of tensile membrane action. In addition, Chung et al. [11] found that the yield load for voided slabs ranged between 96% and 104% of that of solid slabs.

Flexural Stiffness: All investigations noted a flexural stiffness reduction resulted from the presence of voids. Our research, however, reported a 3% stiffness reduction in non-post-tensioned voided slabs and 6% in post-tensioned voided slabs, with the prestressing effect resulting in an approximately 20% increase in stiffness compared to non-prestressed systems. This aligns with Sagadevan & Rao [15], who observed a 6% reduction in flexural stiffness in voided slabs. In contrast, Pawar et al. [10] documented stiffness losses ranging from 5% to 24% with increasing void size. Additionally, Chung et al. [11] further corroborated stiffness losses ranging from 9% to 15%.

5. Conclusions

This study investigated the flexural behavior of prestressed post-tensioned voided biaxial slabs under uniformly distributed loads. The findings reveal that post-tensioning significantly enhances the stiffness and flexural capacity of voided slabs, effectively mitigating the minor stiffness reductions (3–6%) caused by the presence of voids. Notably, post-tensioning increased the stiffness of voided slabs by 21% compared to non-prestressed counterparts.

Post-tensioned voided (PT-Voided) slabs retained 96% of the yield capacity of solid post-tensioned (PT-Solid) slabs while reducing concrete volume by 22%, underscoring their potential for material efficiency. Furthermore, the 6% reduction in stiffness compared to PT-Solid slabs is a modest trade-off, given the significant weight savings achieved. These results suggest that PT-Voided slabs provide a feasible and innovative solution for lightweight yet high-performing structural designs.

A key contribution of this research is the demonstrated superiority of PT-Voided slabs over reinforced concrete voided (RC-Voided) slabs. Post-tensioning delayed the onset of cracking, enhanced stiffness by 21%, and increased the yield load by 41% in PT-Voided slabs compared to RC-Voided slabs. These improvements underscore the efficacy of post-tensioning in compensating for the reduced cross-sectional area caused by voids, enabling PT-Voided slabs to perform comparably to or even surpass solid slabs in critical structural parameters.

Additionally, the prestressed voided slabs exhibited a 22% reduction in weight compared to solid reinforced concrete slabs, which would result in lower seismic loads due to decreased slab weight that represents the mass source in seismic load calculation. This design achieves a self-weight reduction without considerably altering structural performance. Consequently, this self-weight reduction results in decreasing the demands on other structural elements, such as columns and foundations, leading to a decreased need for materials like reinforcement and concrete.

These findings underscore the potential of combining voided slab technology with post-tensioning to achieve an optimal balance between structural efficiency and sustainability.

In addition to the findings presented in this study, a subsequent phase of research is scheduled to undertake an extensive parametric investigation. This forthcoming research will systematically examine the effects of various void configurations and design parameters, including void size, shape, spacing, and reinforcement layout. The aim of this complementary study is to enhance the understanding of the structural performance of prestressed voided slabs under a range of conditions, thereby contributing to the further optimization of their design and application.

Future research should extensively investigate the performance of post-tensioned voided slabs under a variety of loading conditions and other factors. This includes:

Optimization of Void Geometry and Distribution: Exploring various void shapes, sizes, and distributions to identify the configurations that maximize structural efficiency while minimizing material use.

Dynamic Loading: Examining the behavior of post-tensioned voided slabs under dynamic loads, such as those from vehicular traffic, machinery vibrations, and other oscillatory forces, to optimize their design for infrastructure applications.

Seismic Performance: Assessing the seismic resilience of these slabs, particularly their ability to withstand earthquake-induced forces, to ensure their applicability in earthquake-prone regions.

Long-Term Loading: Evaluating the long-term performance and durability of post-tensioned voided slabs under sustained loads and environmental factors like creep, shrinkage, and temperature variations to guarantee their reliability over time.

6. Declarations

6.1. Author Contributions

Conceptualization, A.A.H., M.E.K., and R.T.M.; methodology, A.A.H., M.E.K., and R.T.M.; software, A.A.H.; validation, M.E.K. and R.T.M.; formal analysis, A.A.H.; investigation, A.A.H.; resources, A.A.H.; data curation, A.A.H.; writing—original draft preparation, A.A.H.; writing—review and editing, A.A.H., M.E.K., and R.T.M.; visualization, M.E.K. and R.T.M.; supervision, M.E.K. and R.T.M.; project administration, A.A.H., M.E.K., and R.T.M. All authors have read and agreed to the published version of the manuscript.

6.2. Data Availability Statement

The data presented in this study are available on request from the corresponding author.

6.3. Funding

The authors received no financial support for the research, authorship, and/or publication of this article.

6.4. Conflicts of Interest

The authors declare no conflict of interest.

7. References

[1] Mota, S. (2013). Innovative Structural Slab Practices – Voided Slabs. American Concrete Institute (ACI), Michigan, United States.

[2] Cobiax Technologies. (2010). Cobiax Engineering Manual. Cobiax Technologies AG, Schaffhausen, Switzerland.

[3] BubbleDeck Technology. (2008). BubbleDeck Voided Flat Slab Solutions - Technical Manual and Documents. BubbleDeck Technology, Farum, Denmark.

[4] Daliform Group. (2022). U-Boot Beton - disposable formwork for two-way voided slabs in reinforced concrete cast on site. Daliform Group, Gorgo al Monticano, Italy.

[5] Harding, P. (2004). BubbleDeck–Advanced structure engineering. BubbleDeck Technology, Farum, Denmark.

[6] Jang, S., Melrose, M. D., & Sesil, D. A. (2016). Columbia Medical Center\s Vertical Campus. Proceedings of the Architectural Institute of Korea Conference, 1479-1486.

[7] Anusha, M., Surendra, H. J., Vinod, B. R., & Bhavya, S. (2022). Modelling using finite element analysis in the structural behavior of bubble deck slab. Materials Today: Proceedings, 66, 2397–2404. doi:10.1016/j.matpr.2022.06.337.

[8] Khouzani, M. A, Zeynalian, M., Hashemi, M., Mostofinejad, D., & Farahbod, F. (2020). Study on shear behavior and capacity of biaxial ellipsoidal voided slabs. Structures, 27, 1075–1085. doi:10.1016/j.istruc.2020.07.017.

[9] Sagadevan, R., & Rao, B. N. (2019). Effect of void former shapes on one-way flexural behaviour of biaxial hollow slabs. International Journal of Advanced Structural Engineering, 11(3), 297–307. doi:10.1007/s40091-019-0231-7.

[10] Pawar, A. J., Patil, Y. D., Vesmawala, G. R., Dhake, P. D., & Nikam, J. S. (2024). Investigating the flexural behaviour of biaxial voided slab with varying size and spacing of cuboidal shaped void formers with innovative type of fixing reinforcement. Structures, 64, 106616. doi:10.1016/j.istruc.2024.106616.

[11] Chung, J. H., Jung, H. S., & Choi, H. K. (2022). Flexural Strength and Stiffness of Donut-Type Voided Slab. Applied Sciences (Switzerland), 12(12), 5782. doi:10.3390/app12125782.

[12] Bhamare, V.P., Jadhao, P.D., Pawar, A.J. (2019). Design and Experimental Study of Voided Slab with Proposed New Shape of Void Former. Smart Technologies for Energy, Environment and Sustainable Development. Lecture Notes on Multidisciplinary Industrial Engineering. Springer, Singapore. doi:10.1007/978-981-13-6148-7_51.

[13] Khouzani, M. A., Zeynalian, M., Hashemi, M., Mostofinejad, D., Farahbod, F., & Shahadifar, M. (2021). A numerical study on flexural behavior of biaxial voided slabs containing steel cages. Journal of Building Engineering, 44, 103382. doi:10.1016/j.jobe.2021.103382.

[14] Vinod Kumar, M., & Hamza, T. A. (2020). Finite element analysis on effect of different ball spacing in bubble deck lightweight concrete slab. IOP Conference Series: Materials Science and Engineering, 872(1), 12124. doi:10.1088/1757-899X/872/1/012124.

[15] Sagadevan, R., & Rao, B. N. (2020). Flexural Behavior of Reinforced Concrete Biaxial Voided Square Slabs. ACI Structural Journal, 117(5), 3–14. doi:10.14359/51724664.

[16] Pawar, A. J., Mathew, N. S., Dhake, P. D., & Patil, Y. D. (2022). Flexural behavior of Two-Way voided slab. Materials Today: Proceedings, 65, 1534–1545. doi:10.1016/j.matpr.2022.04.500.

[17] Jain, N., Hussain, A. (2022). Numerical Analysis on Voided Slab with Different Reinforcement on ANSYS 2020R1. I) Advances in Construction Materials and Sustainable Environment. Lecture Notes in Civil Engineering, 196, Springer, Singapore. doi:10.1007/978-981-16-6557-8_41.

[18] Sagadevan, R., & Rao, B. N. (2021). Experimental and analytical investigations on two-way flexural capacity of biaxial voided slab. Structures, 81, 233–247. doi:10.1007/978-981-15-5235-9_18.

[19] Jain, N., & Hussain, A. (2024). Analytical investigation and cost comparison on voided slab using ABAQUS. Asian Journal of Civil Engineering, 25(5), 4121–4132. doi:10.1007/s42107-024-01035-7.

[20] Mahmoudian, A., Mahmoudi, M., Yekrangnia, M., Tajik, N., & Mohammadzadeh Taleshi, M. (2025). A novel machine learning-based approach to determine the reduction factor for punching shear strength capacity of voided concrete slabs. Discover Civil Engineering, 2(1). doi:10.1007/s44290-025-00181-4.

[21] Chung, J. H., Bae, B. Il, Choi, H. K., Jung, H. S., & Choi, C. S. (2018). Evaluation of punching shear strength of voided slabs considering the effect of the ratio b0/d. Engineering Structures, 164, 70–81. doi:10.1016/j.engstruct.2018.02.085.

[22] ACI 318-19. (2019). ACI 318-19 Building Code Requirements for Structural Concrete (ACI 318-19) and Commentary (ACI 318R-19). American Concrete Institute (ACI), Michigan, United States. doi:10.14359/51716937.